Desalination 253 (2010) 38–45

Contents lists available at ScienceDirect

Desalination

journal homepage: www.elsevier.com/locate/desal

Effect of operating conditions and solution chemistry on model parameters in crossflow reverse osmosis of natural organic matter

Supatpong Mattaraj [a,b,*], Wongphaka Phimpha [a], Pakasit Hongthong [a], Ratana Jiraratananon [c]

[a] Environmental Engineering Program, Department of Chemical Engineering, Faculty of Engineering, Ubon Ratchathani University, Ubonratchathani 34190, Thailand
[b] National Center of Excellence for Environmental and Hazardous Waste Management, Ubon Ratchathani University, Ubonratchathani 34190, Thailand
[c] Department of Chemical Engineering, Faculty of Engineering, King Mongkut's University of Technology Thonburi, Bangkok 10140, Thailand

ARTICLE INFO

Article history:
Received 18 August 2009
Received in revised form 19 November 2009
Accepted 27 November 2009
Available online 3 Janaury 2010

Keywords:
Cake resistance
Flux decline
Natural organic matter
Reverse osmosis

ABSTRACT

This paper describes the effect of operating conditions and solution chemistry on model parameters in crossflow reverse osmosis of natural organic matter. Mathematical fouling model based on the combined osmotic pressure and cake filtration model was used to evaluate model parameters (i.e. steady-state flux, J^* and specific cake resistance, α_{cake}). In addition, the empirical equation for steady-state flux ($J^* = 9.12\times10^{-8}\Delta P^{1.04}v^{0.223}R^{-1.18}I^{-0.590}$) was successfully determined to characterize reverse osmosis operation. Steady-state flux increased with increased operating pressure, indicating a pressure-dependent steady-state flux under laminar flow condition. The specific cake resistance ($\alpha_{cake} = 7.943\times10^{12}\Delta P^{-2.03}v^{-0.739}R^{6.29}I^{1.37}$) was inversely related to increased operating pressure and crossflow velocity, while the specific cake resistance increased linearly with recovery effects and ionic strength. Recovery effects with high ionic strength resulted in the highest flux decline, corresponding to high specific cake resistance (i.e. lowering cake porosity) due to combined salt concentration polarization and NOM cake compaction near the membrane surface.

1. Introduction

Reverse osmosis (RO) is the well-known membrane separation process which can be applied for seawater and brackish water desalination, softening, disinfection by-product control, and removal of organics and specific inorganic contaminants such as arsenic, barium, nitrite, nitrate, and other inorganic contaminants [1,2]. The application of membranes has been increasingly used for water treatment in order to control a precursor of the formation of disinfection by-products such as natural organic matter (NOM) during chlorination operation in conventional water treatment [3]. However, fouling of membranes caused by NOM and inorganic salts on the membrane surface can be a major cause of a significant loss of water productivity [4–6].

Membrane fouling can be dependent on membrane characteristics (i.e. pore size, charge, and roughness) [7,8], solution compositions (i.e. humic acid concentration, pH, ionic strength, and calcium concentration) [9,10], and hydrodynamic conditions (i.e. flux, pressure, and crossflow velocity) [10,11]. Fouling can also lead to decreased solution flux due to adsorption/deposition of solute on the membrane surface and in the membrane pores, and cake formation at the membrane surface. Tang et al. [10] indicated that flux reduction during RO of humic acid increased with increasing initial flux (i.e. increased operating pressure), while the tight RO showed less flux decline than the more permeable membranes. Higher operating pressure in NF of humic acids increased flux decline, while higher crossflow velocity increased solution flux due to increased back-transport of solute to the bulk solution, thus decreasing solute accumulation at the membrane surface [12]. Zhu and Elimelech [13] studied the fouling mechanisms during RO of silica colloids. They found that higher permeate flux caused by increasing transmembrane pressure resulted in a greater rate of particle deposition onto membrane surface, and thus an increased rate of membrane fouling. However, previous work showed different results indicating that the specific flux normalized to the initial value was found to be inversely related to the initial permeate rate [14]. The specific resistance of particle deposits on membranes decreased as the initial permeation rate increased, suggesting that cake morphology was an important parameter in determining permeate flux [14]. Kilduff et al. [15] indicated that the rate of flux decline increased with increasing recovery because of the increase of solute concentration on the membrane surface caused by enhancing the convective transport of mass to the membrane surface. Previous studies indicated that the operating conditions could influence membrane performance with different membrane uses and solutions [10], but there is a lack of characterization of model parameters and development of the empirical relationship among membrane operating conditions and solution chemistry.

The objective of this study was to investigate the effects of operating conditions on model parameters (i.e. steady-state flux, J^*

* Corresponding author. Environmental Engineering Program, Department of Chemical Engineering, Faculty of Engineering, Ubon Ratchathani University, Ubonratchathani 34190, Thailand. Tel.: +66 45 353 344; fax: +66 45 353 333.
E-mail addresses: mattas@ubu.ac.th, supatpong.m@hotmail.com (S. Mattaraj).

0011-9164/$ – see front matter © 2009 Elsevier B.V. All rights reserved.
doi:10.1016/j.desal.2009.11.039

and specific cake resistance, α_{cake}) with different ionic strengths during reverse osmosis of natural organic matter and to develop an empirical relationship among membrane operating conditions and solution chemistry. The empirical equations for J^* and α_{cake} were developed with dependent variables for operating pressure (ΔP), crossflow velocity (v), recovery (R), and ionic strength (I). Experimental results exhibited flux decline and rejection with different operating conditions and ionic strengths. The model parameters were determined using the combined osmotic pressure and cake filtration model, while a resistance-in-series model was used to characterize fouling resistances of tight RO system operation. The experimental results of this work could provide an insight evidence for changes in the model parameters as a function of system operating conditions and solution chemistry during crossflow RO.

2. Theory

2.1. Resistance-in-series model

Resistance-in-series model has been widely applied to describe the permeation flux of the membrane processes. This model incorporates membrane hydraulic resistance (R_m) and hydraulic resistances of fouling layer (R_f) on membrane surface. The membrane hydraulic resistance can be determined from the pure water flux without materials deposited on the membrane surface or within the membrane pore by using Darcy's law as shown in Eq. (1).

$$J_o = \frac{1}{A_m}\frac{dV}{dt} = \frac{\Delta P}{\mu R_m} \tag{1}$$

where J_o is the clean water flux (LMH), t is the filtration time (min), V is the permeate volume (L), ΔP is the transmembrane pressure (kPa), A_m is the membrane area (m^2), μ is the dynamic viscosity (kg $m^{-1}s^{-1}$). Eq. (2) accounts for total hydraulic resistance (R_{Total}) due to the combination between membrane hydraulic resistance (R_m) and the hydraulic resistances of fouling layer (R_f) caused by a combination of salt concentration polarization and/or cake formation, and resistant fouling as follows:

$$J_v = \frac{\Delta P - \sigma\Delta\pi}{\mu(R_m + R_f)} = \frac{\Delta P - \sigma\Delta\pi}{\mu(R_m + R_{c1} + R_{c2} + R_{c3} + R_{non-rec})} \tag{2}$$

where J_v is the solution flux (LMH), σ is the osmotic reflection coefficient (−), π is the osmotic pressure (kPa), R_{c1} is the fouling resistance caused by salt concentration polarization and/or cake formation, which can be recovered by hydrodynamic cleaning (m^{-1}), R_{c2} is the recoverable fouling resistance caused by salt layer using acidic cleaning (m^{-1}), R_{c3} is the reversibly adsorbed NOM layer resistance recoverable using alkaline cleaning (m^{-1}), and $R_{non\text{-}rec}$ is the "non-recoverable" resistance ($R_{non\text{-}rec}$) that remains after hydrodynamic and chemical cleaning (m^{-1}).

2.2. Combined osmotic pressure and cake filtration model

The combined osmotic pressure and cake filtration model was previously described by Mattaraj et al. [16]. The model has been previously used to characterize the nanofiltration performance of a solution containing both salt and NOM. The change in solution flux with time is related to the change in osmotic pressure as a result of salt concentration polarization, and the change in the hydraulic resistance of the NOM cake accumulated on the membrane surface as shown below:

$$\frac{dJ_v}{dt} = -\frac{\sigma_s \alpha_s R_{mem,s} \beta_s}{\mu(R_{m,s} + R_{non-rec} + R_c)}\left(\frac{dC_{reten,s}}{dt}\right) - \frac{J_v}{(R_{m,s} + R_{non-rec} + R_c)}\left(\frac{dR_c}{dt}\right) \tag{3}$$

where the subscript s refers to salt species (i.e. NaCl). The first term in the right-handed side describes the osmotic pressure model based on increased salt concentration, while the second term illustrates the additional resistance due to cake formation of NOM accumulation on the membrane surface. In the cake filtration with constant specific cake resistance (α_{cake}), the change in cake resistance with time is related to the rate of change in cake mass, m_{cake} (kg), which equals to the net rate of mass transport towards the membrane surface; i.e., the convective flux, J_v, minus the steady-state flux, J^* (LMH), associated with back-transport resulting from crossflow velocity. Therefore,

$$\frac{dR_c}{dt} = \alpha_{cake}\frac{dm_{cake}}{A_m dt} = \alpha_{cake} C_{reten,NOM}(t)(J_v - J^*) \tag{4}$$

where α_{cake} is the specific cake resistance (m kg^{-1}), $C_{reten,NOM}$ is the NOM concentration in the retentate (kg m^{-3}). Eqs. (3) and (4) can be determined using the fitting model parameters (i.e. steady-state flux, J^* and specific cake resistance, α_{cake}) in a fourth-order Runge–Kutta routine in order to minimize the sum squared errors between the experimental data and estimated data from the combined mathematical fouling model. The fitted model parameters were determined based on 95% confidence interval for non-linear regression described by Draper and Smith [17]. In this work, the combined osmotic pressure and cake filtration model (Eq. (3)) was used to determine model parameters with different operating conditions and ionic strengths.

3. Experimental

3.1. Natural organic matter (NOM)

Natural organic matter (NOM) was obtained from the surface water reservoir at Ubon Ratchathani's University (UBU), Thailand. A polyamide thin-film composite (TFC) reverse osmosis (RO) membrane (model: AG4040F-spiral wound crossflow, GE osmonics, USA) was used to isolate NOM components and subsequently applied the isolated NOM for the crossflow reverse osmosis experiments. The isolation procedure was previously described by Kilduff et al. [18]. The characteristics of natural water were previously described by Jarusutthirak et al. [19]. The isolated NOM and salt were diluted and mixed with deionized water to obtain the required concentrations for both NOM and ionic strengths.

3.2. Crossflow filtration experiments

A bench-scale crossflow test cell with a recycle loop was used for crossflow filtration experiments. A thin-film polyamide reverse osmosis (Model AG 2540F1328 spiral wound crossflow), obtained from GE Osmonics, Inc. USA, was used to investigate membrane performance during filtration experiments. According to manufacturer's information, averaged salt (NaCl) rejection (based on a 2000 mg L^{-1} NaCl solution, pH 7.5, 15% recovery, and 25 °C) is about 99.5% at 1551 kPa. Typical operating pressure is approximately 1379 kPa. The operating pH is in the range of 4–11, while the cleaning pH is in the range of 2–12. The maximum operating temperature is about 45 °C. Membrane sheets were initially cleaned and pre-compacted with deionized water. Clean water flux was determined with a function of operating pressure. After membrane compaction, averaged RO membrane permeability was approximately $1.231\times10^{-8}\pm0.053\times10^{-8}$ m s^{-1} kPa^{-1}(0.0443 LMH kPa^{-1}, number of samples are 17 samples within 95% confidence interval). The membrane hydraulic resistance (R_m) for RO was about 9.39×10^{13} m^{-1}. All filtration experiments were conducted at room temperature at about 26 °C. Membrane sheets were stored in 1% $Na_2S_2O_5$ and kept in a refrigerator at about 4 °C to minimize bacterial activity.

For filtration experiments, NaCl solution contained salt concentration (NaCl) with ionic strengths (I) of 0.01 M and 0.05 M, while feed NOM concentration was maintained at 10 mg L^{-1} with solution pH of 7. System operation was adjusted to achieve an initial solution flux of 30 LMH, while membrane operating pressure was kept constant during filtration experiments. The operating conditions tested included operating pressures (ΔP) in the range of 551.4 to 965 kPa, crossflow velocity (v) in the range of 0.1 to 0.4 m s^{-1}, and recovery ($R = Q_{perm}/Q_{feed}$) in the range of 75 to 95%.

3.3. Analytical methods

Salt concentrations were determined using a conductivity meter (model: inoLab cond Level 2, Germany). Solution pH was measured with pH meter (model: inoLab pH level 1, Wissenschaftlich-Technische Werkstatten, GMBH, Germany). Ionic strength of samples was calculated using a correlation between conductivity and ionic strength; for NaCl standards, I.S.[mol L^{-1}] = $0.5\Sigma C_i Z_i^2 = 9.5\times10^{-6}\times(\mu S\ cm^{-1})$ at 25 °C ($R^2 = 0.999$). NOM concentrations were measured as dissolved organic matter (DOC) using total organic carbon (TOC) analyzer (Shimadzu Corporation, TOC-VCPH model, Japan). Standard solutions were prepared using potassium hydrogen phthalate in deionized water. UV absorbance was measured using a UV–visible spectrophotometer (Shimadzu Corporation, model UV mini 1240, Japan). The weight-averaged molecular weights of NOM were determined using high pressure size exclusion chromatography (HPSEC) (Shimadzu Corporation, model CTO-10Avp, Japan). The procedure was employed as described by Chin et al. [20]. Poly(styrene sulfonate) standards (MW 4300, 6800, 17,000, and 32,000 Da) were used as standard solutions. Low molecular weight standard included benzoic acid (Na^+ form) (MW 122 g/mol), which was detected at wavelength of 254 nm, for standard solution with correlation: log MW = $-0.3702\times t + 7.1471$, $R^2 = 0.987$. NOM mass balance was determined using a series of ultrafiltration membranes including 1, 3, 5, 10, 30, and 100 kDa molecular weight cutoff (MWCO).

3.4. Membrane cleaning

Cleaning procedure included hydrodynamic cleaning followed by chemical cleaning incorporating acidic and alkaline cleaning. First, for hydrodynamic cleaning, deionized water was recirculated in the recycle loop for 30 min at high crossflow velocity of 0.2 to 0.4 m s^{-1}. Deionized water was subsequently used to determine permeate flow as a function of operating pressures. For chemical cleaning, acidic solutions (using citric acid) with pH 4 and followed with alkaline solutions (using sodium hydroxide) with pH of 10 were used to remove inorganic salt and adsorbed NOM with 30-min each for recirculation in the system. Deionized water was further used to measure water flux with different operating pressures. After each cleaning, the water flux as a function of operating pressures was used to determine the recoverable fouling resistances (R_{c1}, R_{c2}, and R_{c3}) and the non-recoverable resistance ($R_{non\text{-}rec}$).

4. Results and discussion

4.1. NOM molecular weight

Fig. 1 shows the NOM molecular size distribution. The response of $UV_{254\ nm}$ was presented in wide range of high molecular weight (10,000–100,000 Da) and low molecular weight (less than 5000 Da). The weight-averaged NOM molecular weight (M_w) was approximately 4144 Da, while the number-averaged NOM molecular weight (M_n) was about 244 Da. The polydispersity of NOM solution (the ratio of the weight- (M_w) to number-averaged (M_n) molecular weights) was approximately 16.98, indicating wide molecular size distribution. NOM was further fractionated using several molecular weights of ultrafiltration (UF). It was found that organic carbons of NOM were approximately 18.6%, 11.1%, 17.9%, 11.5% and 40.9% for less than 1 K, 1–5 K, 5–30 K, 30–100 K, and greater than 100 K UF, respectively. The organic carbon fractions of greater than 5 K were relatively high, more than 70%, indicating higher molecular weight fractions than relatively low molecular weight fractions.

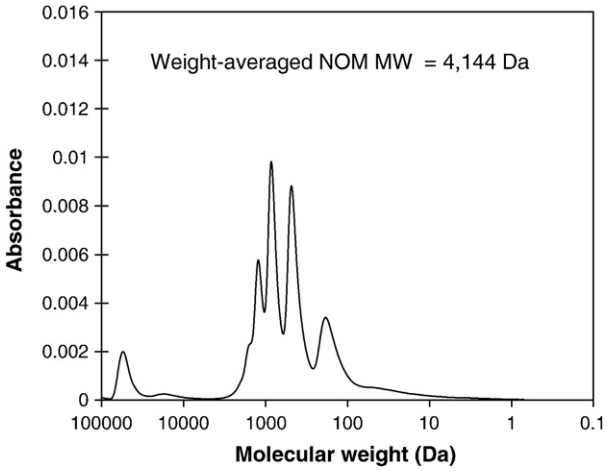

Fig. 1. NOM molecular size distribution.

4.2. Effect of operating pressure on normalized flux and rejection

Fig. 2 presents the effect of operating pressure on normalized flux, while the reverse osmosis performance is tabulated in Table 1. Dot points were the experimental data, while the solid lines were the values obtained from the combined osmotic pressure and cake filtration model (Eq. (3)). Experimental results revealed that increased operating pressures resulted in increased initial solution flux (graph not shown) and significantly increased steady-state solution flux at the end of filtration (as determined within 95% confidence interval shown in Table 1), indicating a pressure-dependent solution flux. Solutions having low operating pressure showed greater flux decline than those having high operating pressure, especially at low ionic strength. At high ionic strength of 0.05 M, the normalized fluxes were slightly increased with operating pressures ranging from 551.4 kPa to 965 kPa, while normalized fluxes of low and high ionic strengths ranged from 0.369 to 0.499 and 0.175 to 0.209, respectively. Fig. 3 illustrates the best fit values of the steady-state flux with a function of operating pressures. The model correlates linearly in the log–log plot with the slopes of 1.134 (1.07,1.205) and 0.96 (0.937,0.987) for low and high ionic strength,

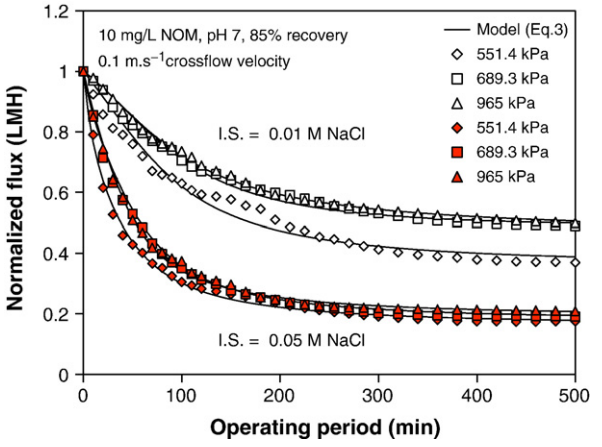

Fig. 2. Effect of operating pressure on normalized flux.

Table 1
Effect of operating pressure on reverse osmosis performance.

Parameters	I.S. = 0.01 M NaCl Operating pressure (kPa)			I.S. = 0.05 M NaCl Operating pressure (kPa)		
	551.4	689.3	965	551.4	689.3	965
J_v/J_{vo} (−)	0.369	0.489	0.499	0.175	0.190	0.209
J^* (m s^{-1})×10^6	2.82 (2.68–2.96)	3.922 (3.84–4.0)	5.371 (5.32–5.421)	1.292 (1.226–1.358)	1.536 (1.506–1.565)	2.2 (2.125–2.275)
$C_{reten,s}$ (M)	0.0569	0.0617	0.0626	0.1179	0.1349	0.1782
$C_{perm,s}$ (M)	0.0033	0.0035	0.0034	0.0341	0.0261	0.0333
$R_{feed,s}$ (%)	68.7	63.7	68.2	36.8	41.0	40.8
$R_{reten,s}$ (%)	94.2	94.3	94.6	71.1	80.7	81.3
$R_{reten,NOM}$ (%)	97.0	97.1	97.0	95.1	95.9	96.4
$R_{m,s}$ (m^{-1})×10^{-14}	2.029	2.159	1.535	2.050	1.564	1.659
$R_{non-rec}$ (m^{-1})×10^{-14}	0.0491	0.0462	0.037	0.0494	0.0639	0.0559
α_{cake} (m kg^{-1})×10^{-17}	3.163 (2.664–3.66)	2.418 (2.151–2.685)	0.826 (0.778–0.874)	18.572 (17.268–19.876)	10.828 (10.565–11.09)	7.31 (6.723–7.898)

The membrane hydraulic resistance (R_m) for RO was about 9.39×10^{13} m^{-1}. The $C_{reten,s}$ and $C_{perm,s}$ are the salt concentration in the retentate and permeate. The $R_{feed,s}$, $R_{reten,s}$ and $R_{reten,NOM}$ are the rejections in the feed and retentate for salt and in the retentate for NOM, respectively. The values in parenthesis indicate the 95% confidence interval for the model parameters.

respectively. The values in the parenthesis indicate the 95% confidence interval for the fitted parameters. Experimental data and calculated results were shown to be in good agreement with high correlation R^2 of greater than 0.98. For both low and high ionic strengths, the averaged salt rejections in the retentate ($R_{reten,s}$) increased from 94.2% to 94.6% and 71.1% to 81.3% with increased operating pressures. The results corresponded to an increased salt concentration in the retentate with operating pressure, while the ratio between the salt concentration in the retentate ($C_{reten,s}$) and in the feed ($C_{feed,s}$) decreased with ionic strength as a continuous removal of salt concentration in the permeate ($C_{perm,s}$) (values shown in Table 1). The reduction in salt rejection at high ionic strength was caused by reduced charge repulsion between negatively charged membrane and positively charged sodium, enhancing decreased double layer thickness at the membrane surface, thus lowering salt rejection [16]. Solution flux in the presence of salt could enhance a reduction in flux decline. This indicated a decreased in membrane permeability, thus increased membrane hydraulic resistance [6]. The membrane hydraulic resistance with the presence of salt can be determined based on the change in solution flux due to increased salt concentration as described by Mattaraj et al. [16]. Salt effects could cause membrane pore structure due to decreased electrostatic repulsion (or charge neutralization at the membrane surface), causing a change in membrane porosity [21]. The membrane hydraulic resistances in the presence of salt ($R_{m,s}$) were in the range of 1.535×10^{14} to 2.159×10^{14} m^{-1}, higher than membrane hydraulic resistances of 9.39×10^{13} m^{-1} (increased by 1.63 to 2.3 times). Based on the combined osmotic pressure and cake filtration model (Eq. (3)), the specific cake resistance (α_{cake}) decreased with increased operating pressures, while the specific cake resistance increased with increased ionic strengths. Chellam and Wiesner [14] indicated that the specific cake resistance of particle deposits on crossflow membrane decreased as the initial permeate rate increased. Increased ionic strengths resulted in an increase of specific cake resistance during nanofiltration of NOM [6,16]. At low operating pressures of 551.4 kPa, the specific cake resistances of low and high ionic strengths were about 3.163×10^{17} m kg^{-1} and 1.857×10^{18} m kg^{-1}, respectively. This indicated that solution flux decreased as a result of the combined salt and NOM accumulation at the membrane surface. The averaged NOM rejections were relatively high in the trend of increased operating pressures about 97% to 97.1% and 95.1% to 96.4% for low and high ionic strength, respectively. The results suggested that RO could possibly remove most organic carbon fractions in NOM components (i.e. large NOM molecular weight), while some organic carbon fractions (i.e. small NOM molecular weights) could pass through the membrane surface depending on solution chemistry (i.e. high ionic strength). Increased ionic strength decreased NOM rejection, possibly due to more compacted NOM configuration (possibly becoming more a rigid, coiled, and spherical) on nanofiltration membrane [6]. The effect of a thin foulant deposit layer may cause significant flux decline through enhanced salt concentration polarization, thus enhancing salt passage through the membrane surface [22]. After hydrodynamic and chemical cleaning, the non-recoverable resistances ($R_{non-rec}$) were relatively low in the range of 3.7×10^{12} m^{-1} to 4.91×10^{12} m^{-1} and 4.94×10^{12} m^{-1} to 6.39×10^{12} m^{-1} for low and high ionic strength, respectively.

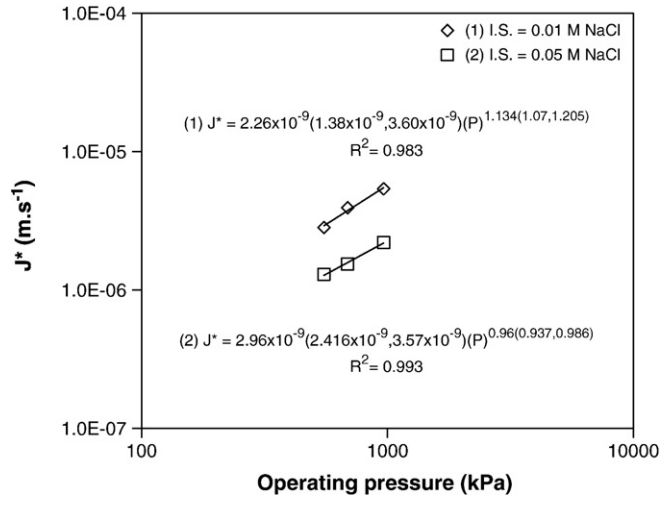

Fig. 3. Best fit values of steady-state flux with a function of operating pressure. The values in parenthesis indicate the 95% confidence interval for the fitted parameters.

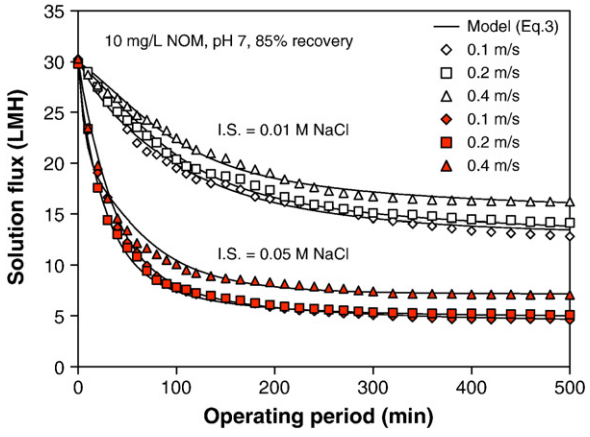

Fig. 4. Effect of crossflow velocity on solution flux.

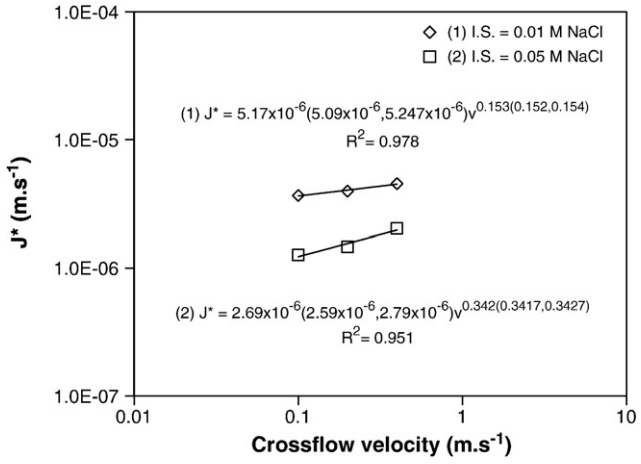

Fig. 5. Best fit values of steady-state flux with a function of crossflow velocity. The values in parenthesis indicate the 95% confidence interval for the fitted parameters.

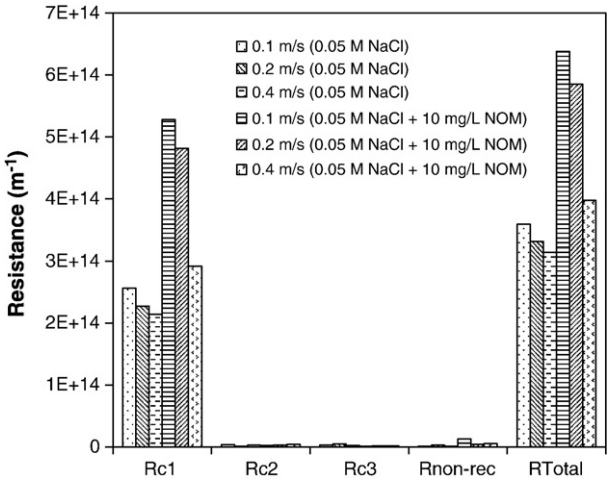

Fig. 6. Resistance parameters due to crossflow velocity effects ($R_m = 0.939\times10^{13}\ m^{-1}$).

4.3. Effect of crossflow velocity on normalized flux and rejection

Fig. 4 exhibits the effect of crossflow velocity on solution flux. The reverse osmosis performance with crossflow velocity effects is shown in Table 1. Increased crossflow velocity showed no significant effect at the initial rate of solution flux, while it enhanced significant effect in flux decline for longer period of filtration. The initial rates of solution flux decline were caused primarily by salt concentration polarization and membrane permeability reduction (i.e. increased membrane hydraulic resistances, $R_{m,s}$). The permeate flux decline of initial stage of colloid crossflow filtration was independent of shear rate [23]. Increased crossflow velocity ranging from 0.1 to 0.4 m s^{-1} increased steady-state solution flux from 3.663×10^{-6} m s^{-1} to 4.531×10^{-6} m s^{-1} and from 1.264×10^{-6} m s^{-1} to 2.031×10^{-6} m s^{-1} for low and high ionic strength, respectively. The results corresponded to decrease in flux decline with increased crossflow velocity, thus decreased solute accumulation swept away from the membrane surface at high crossflow velocity. Fig. 5 shows the best fit values of the steady-state flux with a function of crossflow velocity. The log–log plot between the steady-state flux and crossflow velocity exhibits high correlation with a slope of 0.153 (0.152,0.154) and 0.342 (0.3417,0.3427) for low and high ionic strength, respectively. The results suggested system operation in the range of laminar flow condition, previously described by Cheryan [24]. Based on the combined osmotic pressure and cake filtration model, the specific cake resistances (α_{cake}) at low ionic strength of 0.01 M NaCl decreased from 2.484×10^{17} m kg^{-1} to 0.414×10^{17} m kg^{-1} with increasing crossflow velocity. Similar trend was found for solutions having high ionic strength, indicating greater specific cake resistances than those having low ionic strength. Increased salt concentration could reduce charge repulsion at the membrane surface, thus increased $R_{m,s}$ and lowered salt rejection ($R_{reten,s}$) (data shown in Table 2). Salt concentration could present in the cake layer possibly reduced charge repulsion between ionized functional groups on single NOM molecule and between NOM molecules. The results in more compact configuration and NOM cake, suggesting in lower cake porosity. The specific cake resistances described by the Carman–Kozeny equation can be written in terms of cake porosity (ε_{cake}) (−), density (ρ) (kg m^{-3}), and particle diameter (d_p) (m) [25].

$$\alpha_{cake} = \left(\frac{180(1-\epsilon_{cake})^2}{\rho d_p^2 \epsilon_{cake}^3}\right) \quad (5)$$

The above equation indicates that the specific cake resistance is inversely related to ε_{cake}^3 and is linearly corresponded to $(1-\varepsilon_{cake})^2$. Therefore, the equation predicts that decreases in cake porosity result in an increase in the specific cake resistance due to increased NOM cake compaction with the presence of high salt concentration.

A resistance-in-series model was used to determine fouling resistances after hydrodynamic and chemical cleaning. Fig. 6 presents the resistance parameters due to crossflow velocity effects. In the absence of NOM (solution flux not shown), the increased recoverable fouling resistances (R_{c1}) were caused by increased salt concentration polarization, while the combined effects of salt concentration and compacted NOM cake enhanced relatively high in recoverable fouling resistances. It was observed that the recoverable fouling resistance (R_{c1}) decreased from 5.27×10^{14} m^{-1} to 2.92×10^{14} m^{-1} with increased crossflow velocity. The parameter showed greater values than other

Table 2
Effect of crossflow velocity on reverse osmosis performance.

Parameters	I.S. = 0.01 M NaCl Crossflow (m s^{-1})			I.S. = 0.05 M NaCl Crossflow (m s^{-1})		
	0.1	0.2	0.4	0.1	0.2	0.4
J_v/J_{vo} (−)	0.429	0.473	0.540	0.152	0.171	0.234
J^* (m s^{-1})×10^6	3.663 (3.615–3.712)	3.964 (3.906–4.023)	4.531 (4.465–4.596)	1.264 (1.211–1.317)	1.46 (1.431–1.49)	2.031 (1.945–2.118)
$C_{reten,s}$ (M)	0.0561	0.0572	0.0597	0.1316	0.1376	0.1325
$C_{perm,s}$ (M)	0.0036	0.0038	0.0035	0.0309	0.0291	0.0360
$R_{feed,s}$ (%)	67.9	64.0	64.2	39.7	42.7	36.1
$R_{reten,s}$ (%)	93.6	93.4	94.1	76.5	78.9	72.8
$R_{reten,NOM}$ (%)	95.2	95.3	96.2	94.5	95.4	95.2
$R_{m,s}$ (m^{-1})×10^{-14}	2.081	1.109	1.069	1.321	1.093	1.339
$R_{non\text{-}rec}$ (m^{-1})×10^{-14}	0.0375	0.0501	0.011	0.1312	0.0462	0.0529
α_{cake} (m kg^{-1})×10^{-17}	2.484 (2.335–2633)	0.681 (0.574–0789)	0.414 (0.345–0.483)	17.545 (17.065–18.02)	14.33 (13.49–15.174)	13.94 (12.69–15.18)

The membrane hydraulic resistance (R_m) for RO was about 9.39×10^{13} m^{-1}. Initial solution flux is about 30 LMH. The values in parenthesis indicate the 95% confidence interval for the model parameters.

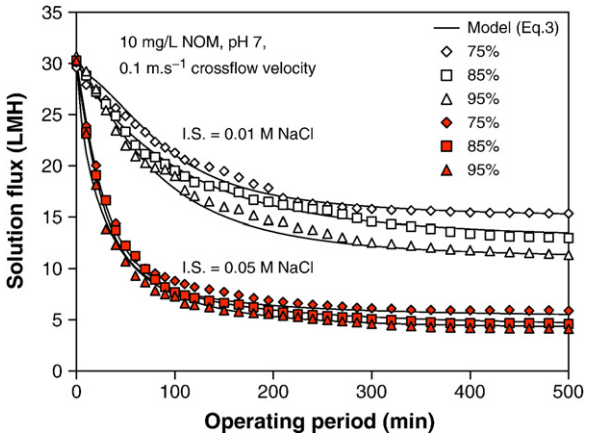

Fig. 7. Effect of recovery on solution flux.

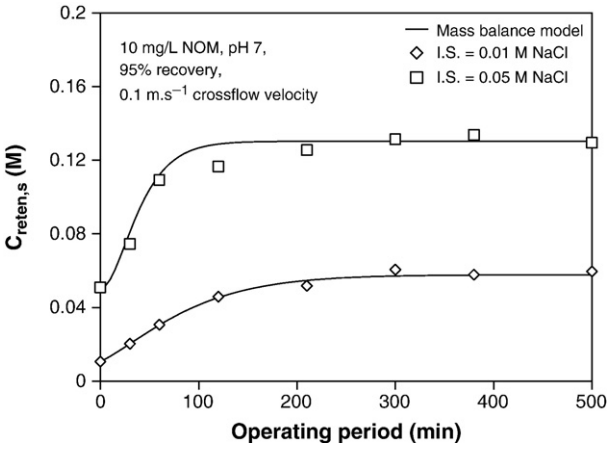

Fig. 8. Effect of ionic strength on salt concentration in the retentate ($C_{reten,s}$).

resistance parameters (R_{c2}, R_{c3}, and $R_{non\text{-}rec}$) ranging relatively low from 1.1×10^{12} to 5.44×10^{12} m^{-1}. System cleaning (i.e. hydrodynamic and chemical cleaning) could effectively remove salt concentration and adsorbed NOM components from the membrane surface and/or pores, suggesting less fouling resistances from the membrane surface due to large NOM molecular weight fractions removed with relatively high NOM rejection.

4.4. Effect of recovery on normalized flux and rejection

Fig. 7 illustrates the effect of recovery on solution flux. The reverse osmosis performance is tabulated in Table 3. Increased recovery from 75% to 95% resulted in greater flux decline, possibly caused by increased solute accumulation at the membrane surface. Solution flux decline was more pronounced at the highest recovery of 95%. Solutions having high ionic strength of 0.05 M NaCl showed greater flux decline than those having low ionic strength of 0.01 M NaCl. With increasing recovery from 75% to 95%, normalized flux decreased from 0.519 to 0.369 and 0.195 to 0.136 for low and high ionic strength, respectively. The rate of flux decline increased with increasing recovery because of the increase of solute concentration on the membrane surface caused by enhancing the convective transport of mass to the membrane surface [15]. The salt rejections in the retentate ($R_{reten,s}$) decreased with increasing recovery as a result of increased salt concentration at the membrane surface. Averaged salt rejections decreased from 93.4%–94.6% to 72.6%–81.2% with increased ionic strengths, while averaged NOM rejections were relatively high ranging from 94.4% to 95.9% (possibly due to large molecular weight fractions). Fig. 8 shows the effect of ionic strength on salt concentration in the retentate ($C_{reten,s}$). Dot points represent the experimental results during filtration experiments, while solid lines demonstrate the mathematical model from mass balance equation, previously studied by Mattaraj et al. [16]. From this figure, solutions having high ionic strength of 0.05 M NaCl showed greater values than those having low ionic strength of 0.01 M NaCl. The steady-state salt concentrations for high ionic strength exhibited greater values (about 2.2 times) than those for low ionic strength. Recovery effects can enhance NOM concentration on the membrane surface, suggesting increased specific cake resistances. Increased recovery from 75% to 95% increased specific cake resistances from 1.02×10^{17} m kg^{-1} to 4.405×10^{17} m kg^{-1} and 7.222×10^{17} m kg^{-1} to 3.242×10^{18} m kg^{-1} for low and high ionic strengths, respectively. The specific cake resistance was the highest values at high ionic strength of 0.05 M NaCl at high recovery of 95%. The results suggested the combined effects of salt concentration and NOM accumulation by adopting more compacted NOM molecules at the membrane surface. Fig. 9 presents the best fit values of specific cake resistance (α_{cake}) with a function of recovery. The correlation was found to be in good agreement with relatively high correlation (R^2>0.99). The slopes of the graph were ranged from 6.207(5.728,6.812) to 6.367(6.118,6.577) with 95% confidence interval. After system cleaning, the non-recoverable resistances ($R_{non\text{-}rec}$) showed relatively high at high ionic strength of 0.05 M NaCl, when compared the values with low ionic strength. This suggested that NOM cake accumulation could result in a highly compacted fouling layer at the membrane surface.

4.5. Relationship among operating conditions and ionic strengths on model parameters

Membrane system operation and solution chemistry could significantly affect reverse osmosis performance and model parameters (i.e.

Table 3
Effect of recovery on reverse osmosis performance.

Parameters	I.S. = 0.01 M NaCl Recovery (%)			I.S. = 0.05 M NaCl Recovery (%)		
	75	85	95	75	85	95
J_v/J_{vo} (−)	0.519	0.429	0.369	0.195	0.152	0.136
J^* (m s^{-1})×10^6	4.289 (4.181–4.396)	3.663 (3.615–3.712)	3.188 (3.144–3.233)	1.542 (1.502–1.583)	1.264 (1.211–1.317)	1.194 (1.136–1.252)
$C_{reten,s}$ (M)	0.0569	0.0561	0.0575	0.1302	0.1316	0.129
$C_{perm,s}$ (M)	0.0031	0.0036	0.0038	0.0245	0.0309	0.0354
$R_{feed,s}$ (%)	70.3	67.9	64.1	49.3	39.7	30.4
$R_{reten,s}$ (%)	94.6	93.6	93.4	81.2	76.5	72.6
$R_{reten,NOM}$ (%)	95.9	95.2	95.0	95.7	94.5	194.4
$R_{m,s}$ (m^{-1})×10^{-14}	1.179	2.081	0.9834	1.025	1.321	1.457
$R_{non\text{-}rec}$ (m^{-1})×10^{-14}	0.0033	0.0375	0.0396	0.9046	0.1312	0.9090
α_{cake} (m kg^{-1})×10^{-17}	1.0201 (0.84–1.20)	2.484 (2.335–2.633)	4.405 (4.175–4.635)	7.222 (6.81–7.633)	17.545 (17.065–18.02)	32.415 (28.75–36.08)

The membrane hydraulic resistance (R_m) for RO was about 9.39×10^{13} m^{-1}. Initial solution flux is about 30 LMH. The values in parenthesis indicate the 95% confidence interval for the model parameters.

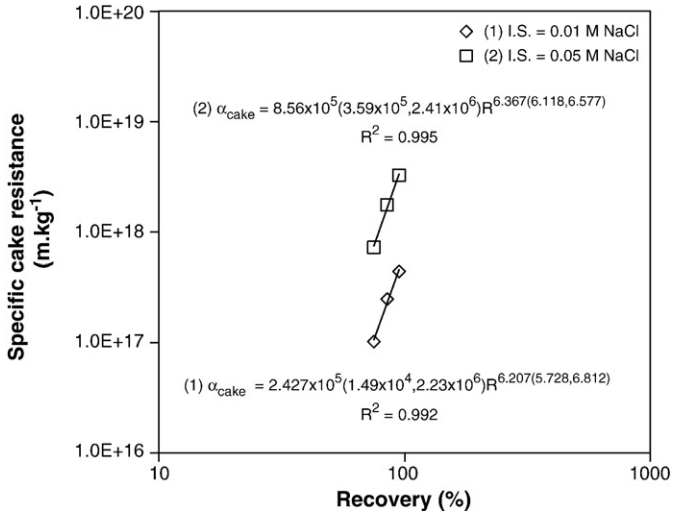

Fig. 9. Best fit values of specific cake resistance (α_{cake}) with a function of recovery. The values in parenthesis indicate the 95% confidence interval for the fitted parameters.

steady-state flux, J^* and specific cake resistance, α_{cake}), which were evaluated based on the combined osmotic pressure and cake filtration model (Eq. (3)). The steady-state fluxes and specific cake resistances were previously characterized to depend on membrane operating pressure (ΔP), crossflow velocity (v), recovery (R), and feed ionic strength (I), while solution pH of 7 and NOM concentration of 10 mg L^{-1} were maintained constant for all filtration experiments. The fouling in membrane pores caused by NOM molecular size was assumed to be less significant effect due to tight RO membrane with relatively high NOM rejection and low non-recoverable fouling ($R_{non\text{-}rec}$). The model parameters can be determined using an empirical relationship with a function of operating conditions and ionic strength ($J^* = a\Delta P^b v^c R^d I^e$, where a, b, c, d, and e are the empirical constants). This empirical relationship can be rearranged in the log–log scale as follows:

$$\log J^* = \log a + b\log\Delta P + c\log v + d\log R + e\log I. \quad (6)$$

A multiple linear regression using $\log J^*$ (m s^{-1}) as the dependent variable and $\log \Delta P$ (kPa), $\log v$ (m s^{-1}), $\log R$ (−) and $\log I$ (M) as the dependent variables produces an intercept [equal to $\log a$] and slopes equal to b, c, d, and e. Based on the statistical analysis on experimental data, the empirical equation can be written as follow:

$$J^* = 9.12\times10^{-8}\Delta P^{1.04} v^{0.223} R^{-1.18} I^{-0.590} (R^2 = 0.989). \quad (7)$$

The slopes for operating pressure, crossflow velocity, recovery, and ionic strength are 1.04, 0.223, −1.18, and −0.590, respectively. The correlation coefficient is relatively high with R^2 of 0.989. The 95% confidence interval for a, b, c, d, and e ranged from (7.762×10^{-8},1.072×10^{-7}), (1.01,1.08), (0.219,0.229), (−1.16,−1.21), and (−0.58,−0.601), respectively. The negative values indicate a decreased steady-state flux with recovery ($d=-1.18$) and ionic strength ($e=-0.590$), while the positive values suggest an increased in steady-state flux with operating pressure ($b=1.04$) and crossflow velocity ($c=0.223$). The empirical constants (b) and (c) indicate a pressure-dependent steady-state flux and system operation under laminar flow condition, respectively. Recovery effect and ionic strength showed the worst flux decline, indicating negative values for empirical constants. Increased high ionic strength resulted in a reduction of electrostatic charge repulsion (reducing charge interaction between a negatively charged NOM macromolecule and positively charged salt, thus causing a densely packed cake layer, NOM accumulation and increasing permeate flow resistance) [26].

Specific cake resistance, α_{cake}, (m kg^{-1}) obtained from Eq. (3) can be developed with a function of operating condition and ionic strength ($\alpha_{cake} = f\Delta P^g v^h R^i I^j$, where f, g, h, i, and j are the empirical constants). The statistical analysis with multiple linear regressions can be successfully used to evaluate empirical constants in the log–log scale relationship. The empirical equation of specific cake resistance can be written as follows:

$$\alpha_{cake} = 7.943\times10^{12}\Delta P^{-2.03} v^{-0.739} R^{6.29} I^{1.37} (R^2 = 0.94). \quad (8)$$

The 95% confidence interval for f is in the range of 1.995×10^{12} and 1.585×10^{13}. The slopes for g, h, i, and j are −2.03(−1.98,−2.07), −0.739(−0.706,−0.779), 6.29(6.15,6.47), and 1.37(1.34,1.41), respectively. The values in parenthesis were determined within 95% confidence interval. The correlation coefficient is relatively high with R^2 of 0.94. The results showed negative values for operating pressures ($g=-2.03$) and crossflow velocity ($h=-0.739$), indicating decreased specific cake resistances. Similar observation was observed by Chellam and Wiesner [14]. They indicated that the specific resistance of particle deposits on membranes decreased as the initial permeation rate increased [14]. The increase in α_{cake} can be observed with positive values of recovery ($i=6.29$) and ionic strength ($j=1.37$). The results corresponded to the highest specific cake resistance with solutions having high ionic strength at recovery of 95%. Both empirical equations with combined operating conditions and feed solution chemistry can be successfully determined to interpret reverse osmosis performance.

5. Conclusions

The performance of crossflow reverse osmosis process of NOM with different solution chemistry was analyzed using resistance-in-series model, the combined osmotic and cake filtration model, and the empirical model. The empirical equations for steady-state flux (J^*) and specific cake resistances (α_{cake}) were successfully developed with combined dependent variables of operating pressure (ΔP), crossflow velocity (v), recovery (R). Steady-state flux increased with increased operating pressure and crossflow velocity, while the flux decreased with increased recovery effects and ionic strength. The experimental results indicated a pressure-dependent steady-state flux under laminar flow condition. Flux decline at the initial stage of filtration was due to salt concentration polarization affecting membrane permeability reduction. The specific cake resistance was inversely related to increased operating pressure and crossflow velocity ($\alpha_{cake} = 7.943\times10^{12}\Delta P^{-2.03} v^{-0.739} R^{6.29} I^{1.37}$), while the specific cake resistance increased linearly with recovery effects and ionic strength. Recovery with high ionic strength resulted in the significant flux decline, thus increased specific cake resistance (i.e. lowering cake porosity) due to combined salt concentration polarization and NOM cake compaction near the membrane surface.

Nomenclature

a to j	empirical constants
A_m	membrane area (m^2)
$C_{feed,s}$	salt concentration in the feed (mol L^{-1})
$C_{perm,s}$	salt concentration in the permeate (mol L^{-1})
$C_{reten,NOM}$	NOM concentration in the retentate (kg m^{-3})
$C_{reten,s}$	salt concentration in the retentate (mol L^{-1})
d_p	particle diameter (m)
I	ionic strength (M)
J_o	clean water flux (L $m^{-2}h^{-1}$, LMH)
J_v	solution flux (L $m^{-2}h^{-1}$, LMH)
J^*	steady-state flux associated with back-transport resulting from crossflow (LMH)
m_{cake}	cake mass (kg)
M_n	number-averaged NOM molecular weight (Da)
M_w	weight-averaged NOM molecular weight (Da)

ΔP transmembrane pressure (kPa)
Q_{feed} flow in the feed (mL min^{-1})
Q_{perm} flow in the permeate (mL min^{-1})
R recovery (−)
R_c cake resistance (m^{-1})
R_{c1} fouling resistance by concentration polarization and/or cake formation (m^{-1})
R_{c2} recoverable resistant fouling caused by salt layer (m^{-1})
R_{c3} reversibly adsorbed NOM layer resistance (m^{-1})
R_f hydraulic resistance of fouling layer (m^{-1})
$R_{feed,s}$ salt rejection in the feed (−)
R_m membrane hydraulic resistance (m^{-1})
$R_{m,s}$ membrane resistance in the presence of salt (m^{-1})
$R_{non\text{-}rec}$ non-recoverable resistance (m^{-1})
$R_{reten,s}$ rejection in the retentate for salt (−)
$R_{reten,NOM}$ rejection in the retentate for NOM (−)
R_{Total} total hydraulic resistance (m^{-1})
t operating time (min)
v crossflow velocity (m s^{-1})
V permeate volume (L)

Greek letters

α_s correlation between osmotic pressure and salt concentration (kPa L mol^{-1})
α_{cake} specific cake resistance (m kg^{-1})
β_s salt concentration polarization (−)
ε_{cake} cake porosity (−)
ρ density (kg m^{-3})
μ dynamic viscosity (kg m^{-1} s^{-1})
π osmotic pressure (kPa)
σ osmotic reflection coefficient (−)

Acknowledgements

The authors would like to thank the Thailand Research Fund (TRF) for TRF senior research scholar grant (No. RTA5080014) and the Commission on Higher Education, Thailand, for financial support. We also would like to thank the Department of Chemical Engineering, Faculty of Engineering, Ubon Rachathani University, and the National Center of Excellence for Environmental and Hazardous Waste Management, Ubon Ratchathani University, Ubonratchathani, Thailand, for all experimental equipments applied in this research.

References

[1] F. Wang, V.V. Tarabara, Coupled effects of colloidal deposition and salt concentration polarization on reverse osmosis membrane performance, J. Membr. Sci. 293 (2007) 111–123.
[2] R. Molinari, P. Argurio, L. Romeo, Studies on interactions between membranes (RO and NF) and pollutants (SiO_2, NO_3^-, Mn^{++}, and humic acid) in water, Desalination 138 (2001) 271–281.
[3] A.I. Schafer, A.G. Fane, T.D. Waite, Fouling effects on rejection in the membrane filtration of natural waters, Desalination 131 (2000) 215–224.
[4] W. Yuan, A.L. Zydney, Effects of solution environment on humic acid fouling during microfiltration, Desalination 122 (1999) 63–76.
[5] J. Cho, G. Amy, J. Pellegrino, Membrane filtration of natural organic matter: initial comparison of rejection and flux decline characteristics with ultrafiltration and nanofiltration membranes, Water Res. 33 (1999) 2517–2526.
[6] J.E. Kilduff, S. Mattaraj, G. Belfort, Flux decline during nanofiltration of naturally-occurring dissolved organic matter: effects of osmotic pressure, membrane permeability, and cake formation, J. Membr. Sci. 239 (1) (2004) 39–53.
[7] M. Elimelech, X. Zhu, A.E. Childress, S. Hong, Role of membrane surface morphology in colloidal fouling of cellulose acetate and composite aromatic polyamide reverse osmosis membranes, J. Membr. Sci. 127 (1997) 101–109.
[8] A.R. Costa, M.N. de Pinho, Effect of membrane pore size and solution chemistry on the ultrafiltration of humic substances solutions, J. Membr. Sci. 255 (2005) 49–56.
[9] A.I. Schafer, A. Pihlajamaki, A.G. Fane, T.D. Waite, M. Nystrom, Natural organic matter removal by nanofiltration: effects of solution chemistry on retention of low molar mass acids versus bulk organic matter, J. Membr. Sci. 242 (2004) 73–85.
[10] C.Y. Tang, Y.-N. Kwon, J.O. Leckie, Fouling of reverse osmosis and nanofiltration membranes by humic acid—effects of solution composition and hydrodynamic conditions, J. Membr. Sci. 290 (2007) 86–94.
[11] L. Paugam, S. Taha, G. Dorange, P. Jaouen, F. Quemeneur, Mechanism of nitrate ions transfer in nanofiltration depending on pressure, pH, concentration, and medium composition, J. Membr. Sci. 231 (2004) 37–46.
[12] Z. Wang, Y. Zhao, J. Wang, S. Wang, Studies on nanofiltration membrane fouling in the treatment of water solutions containing humic acids, Desalination 178 (2005) 171–178.
[13] X. Zhu, M. Elimelech, Colloidal fouling of reverse osmosis membranes: measurements and fouling mechanisms, Environ. Sci. Technol. 31 (1997) 3654–3662.
[14] S. Chellam, M.R. Wiesner, Particle back-transport and permeate flux behavior in crossflow membrane filters, Environ. Sci. Technol. 31 (1997) 819–824.
[15] J.E. Kilduff, S. Mattaraj, M. Zhou, G. Belfort, Kinetics of membrane flux decline: the role of natural colloids and mitigation via membrane surface modification, J. Nanopart. Res. 7 (2005) 525–544.
[16] S. Mattaraj, C. Jarausutthirak, R. Jiraratananon, A combined osmotic pressure and cake filtration model for crossflow nanofiltration of natural organic matter, J. Membr. Sci. 322 (2008) 475–483.
[17] N.R. Draper, H. Smith, Applied Regression Analysis, 3rd editionWiley Interscience0-471-17082-8, 1998.
[18] J.E. Kilduff, S. Mattaraj, A. Wigton, M. Kitis, T. Karanfil, Effects of reverse osmosis isolation on reactivity of naturally occurring dissolved organic matter in physicochemical processes, Water Res. 38 (4) (2004) 1026–1036.
[19] C. Jarusutthirak, S. Mattaraj, R. Jiraratananon, Factors affecting nanofiltration performances in natural organic matter rejection and flux decline, Sep. Purif. Technol. 58 (2007) 68–75.
[20] Y.-P. Chin, G. Aiken, E. O'Loughlin, Molecular weight, polydispersity, and spectroscopic properties of aquatic humic substances, Environ. Sci. Technol. 28 (1994) (1994) 1853–1858.
[21] M.R. Teixeira, M.J. Rosa, M. Nystrom, The role of membrane charge on nanofiltration performance, J. Membr. Sci. 265 (2005) 160–166.
[22] E.M.V. Hoek, M. Elimelech, Cake-enhanced concentration polarization: a new fouling mechanism for salt-rejecting membranes, Environ. Sci. Technol. 37 (2003) 5581–5588.
[23] S. Hong, R.S. Faibish, M. Elimelech, Kinetics of permeate flux decline in crossflow membrane filtration of colloidal suspensions, J. Colloid Interface Sci. 196 (1997) 267–277.
[24] M. Cheryan, Ultrafiltration and Microfiltration Handbook, Technomic Publishing Co., Inc., Lancaster, PA, 1998.
[25] M.R. Wiesner, P. Aptel, Mass transport and permeate flux and fouling in pressure-driven processes, in: J. Mallevialle, P.E. Odendaal, M.R. Wiesner (Eds.), Water Treatment Membrane Processes, McGraw-Hill, New York, 2009, ISBN 0-07-0019-7-00151996.
[26] A. Braghetta, F.A. DiGiano, W.P. Ball, NOM accumulation at NF membrane surface: impact of chemistry and shear, J. Environ. Eng. ASCE 124 (11) (1998) 1087–1098.